

Rotating Neutron stars with Quark cores

Ishfaq A. Rather^{1,*}, Usuf Rahaman¹, M. Imran¹, H. C. Das^{2,3}, A. A. Usmani¹, and S. K. Patra^{2,3}

¹*Department of Physics, Aligarh Muslim University, Aligarh 202002, India*

²*Institute of Physics, Bhubaneswar 751005, India and*

³*Homi Bhabha National Institute, Training School Complex, Anushakti Nagar, Mumbai 400094, India*

The rotating neutron star properties are studied with a phase transition to quark matter. The density-dependent relativistic mean-field model (DD-RMF) is employed to study the hadron matter, while the Vector-Enhanced Bag model (vBag) model is used to study the quark matter. The star matter properties like mass, radius, the moment of inertia, rotational frequency, Kerr parameter, and other important quantities are studied to see the effect on quark matter. The maximum mass of rotating neutron star with DD-LZ1 and DD-MEX parameter sets is found to be around $3M_{\odot}$ for pure hadronic phase and decreases to a value around $2.6M_{\odot}$ with phase transition to quark matter, which satisfies the recent GW190814 constraints. For DDV, DDVT, and DDVTD parameter sets, the maximum mass decreases to satisfy the $2M_{\odot}$. The moment of inertia calculated for various DD-RMF parameter sets decreases with the increasing mass satisfying constraints from various measurements. Other important quantities calculated also vary with the bag constant and hence show that the presence of quarks inside neutron stars can also allow us to constraint these quantities to determine a proper EoS. Also, the theoretical study along with the accurate measurement of uniformly rotating neutron star properties may offer some valuable information concerning the high-density part of the equation of state.

I. INTRODUCTION

The compact objects like neutron stars in the known universe are the ideal sources to study the properties and composition of high dense matter. The measurement of mass and the radius for spherically symmetric and static stars impose constraints on the properties of matter at high density. The study of rotating neutron star properties may lead to significant new constraints. From the past decade, the successful discoveries of various gravitational waves by LIGO and Virgo collaborations have allowed us to study the dense matter properties with more constraints imposed on the neutron star Equation of State (EoS). The measurement of tidal deformability for static neutron stars ruled out many EoSs with either too large or too small maximum mass.

The Binary Neutron star (BNS) merger event GW170817 [1, 2] constrained the maximum mass and the tidal deformability of neutron stars and hence on the EoS. The total mass of the GW170817 event was around $2.7M_{\odot}$ with the heavier component mass $1.16\text{--}1.60M_{\odot}$ for low spin priors. The maximum mass approached $1.9M_{\odot}$ for high spin priors [3]. The tidal deformability dependence on the NS radius $\Lambda \propto R^5$ provided a more strong constraint on the high dense nuclear EoS. A new gravitational wave event was observed recently by LVC as GW190814 [4] with a black hole merger of mass $22.2\text{--}24.3M_{\odot}$ and a massive secondary component of mass $2.50\text{--}2.67M_{\odot}$. The secondary component of GW190814 gained a lot of attention about its nature whether it is a black hole, or a neutron star, or some other exotic object [5–15].

The maximum mass of a neutron star is assumed to be the most important parameter determining the

possible outcome of a BNS merger [16–24]. Also, proper knowledge of a neutron star maximum mass and radius constraints the EoS at high density [25–29]. The precise measurement of masses of millisecond pulsars like PSR J1614-2230 (1.928 ± 0.017) M_{\odot} [30], PSR J0348+0432 (2.01 ± 0.04) M_{\odot} [31], and PSR J0740+6620 ($2.04^{+0.10}_{-0.09}$) M_{\odot} [32] show that the theoretical maximum mass of a neutron star should be around $2M_{\odot}$. The $2.3M_{\odot}$ of GW170817 is interpreted as possibly an upper limit on the NS maximum mass [33–35]. However, with the secondary component of GW190814 predicting a maximum mass around $2.5M_{\odot}$, the maximum mass limit for neutron star seems to be weakly constrained.

The effect of EoS on the properties of rotating neutron stars has been studied since the late 90s by various groups [35–38]. To investigate the neutron star structure and its properties, the choice of EoS becomes the starting point. There proper choice of EoS for neutron stars matter invites theoretical discussions. Every single EoS produces a neutron star with different properties. Despite predicting several neutron star properties, the composition at several times the normal nuclear density is still not known properly. The core of a neutron star is considered to be a nuclear matter in β -equilibrium and charge-neutral conditions. Neutron, proton, electron, and muon are the basic components of the core of a neutron star. The neutron star structure with several exotic degrees of freedom like quarks, kaons, and hyperons are also studied [8, 39–42]. The presence of such exotic phases affects the neutron star properties significantly.

The neutron star matter containing only hadrons is studied employing different model parameters at high densities. The Density functional theories (DFT) have been widely used to determine the saturation properties of high dense nuclear matter [43–48]. At saturation density, the nuclear matter EoS is well constrained. The nuclear matter properties are determined with less uncer-

* ishfaqrather81@gmail.com

tainty. These EoSs at several times the normal nuclear density describe the neutron star properties. The relativistic mean-field (RMF) model has been very successful in describing both finite and infinite nuclear matter[49]. The basic mechanism involves the interaction of nucleons via mesons. Different mesons like ρ , σ , ω , δ have reduced the large uncertainties present in the nuclear matter properties and constrained the nuclear matter properties to well within the limits [50–56]. The RMF Equation of states like NL3 [60] and BigApple [13, 61] determine neutron stars with a maximum mass in the range 2.6-2.7 M_{\odot} . The density-dependent RMF (DD-RMF) model contains the density-dependent coupling constants replacing the self-and cross-coupling of various mesons in the basic RMF model [57]. DD-RMF parameters like DD-ME1 [58], DD-ME2 [59] generate very massive neutron stars with a 2.3-2.5 M_{\odot} maximum mass. Several new DD-RMF parameter sets were proposed recently like DD-LZ1[62], DD-MEX [63], DDV, DDVT, and DDVTD [64]. These recently proposed parameter sets are divided into two categories. The DD-LZ1 and DD-MEX parameter sets produce very stiff EoS and hence a large NS maximum mass, belong to the stiff EoS group. Parameter sets like DDV, DDVT, and DDVTD produce soft EoS and hence lie in the softer EoS group. Both the stiff and the soft EoS groups are used in the current study to determine the neutron star properties for the static and rotating case.

The exotic degrees of freedom like quarks have been studied over the past decade. The presence of quarks in the core of neutron stars at very high densities has been proposed [29]. Thus the phase transition to the quark matter inside neutron stars is possible at very high density [65, 66]. A neutron star with hadrons in the core followed by a phase transition to the quark matter at several times the normal nuclear density is termed as the Hybrid star [46, 67–70].

The MIT Bag model [66, 71, 72] was first proposed to study the strange and hybrid stars. The Nambu-Jona-Lasinio (NJL) model [73–77] was later introduced which explained the quark matter more precisely than the bag model. The modified NJL models have been very successful in explaining the stable HSs and also satisfying the recent GW170817 constraints [78, 79]. The modified Bag model, termed as Vector-Enhanced Bag model (vBag) [80] was introduced as an effective model to study the astrophysical processes. The vBag model is favored over the simple bag model and NJL model as it accounts for the repulsive vector interactions along with the Dynamic Chiral Symmetry Breaking (D χ SB). The repulsive vector interaction and the deconfinement for the construction of a mixed-phase allowed it to describe the strange/hybrid stars which attain the 2 M_{\odot} limit.

In the present work, we study the properties of the rotating neutron stars by considering a phase transition from hadron matter to quark matter. The star matter

properties like mass, radius, the moment of inertia, Kerr parameter are studied along with some other important properties. The dependence of these quantities on the neutron star mass is discussed. Several properties of a static star like mass, radius, and tidal deformability are also discussed.

This article is organized as follows: the DD-RMF model for hadron matter and vBag model for quark matter and the phase transition properties are discussed in section(II). The static and rotating neutron structure and various properties associated with the star matter are discussed in sec.III. In sec. (IV), the parameter sets for the nuclear matter and the saturation density properties are defined. The EoS for the hadronic and hybrid star configurations are explained. The static and rotating neutron star properties like mass, radius, the moment of inertia are discussed in subsection(IV.3). Finally, the summary and concluding remarks are given in sec. (V).

II. THEORY AND FORMALISM

The Relativistic Mean-Field (RMF) Lagrangian involves the interaction between the nucleons through various mesons defined as Dirac particles. The most basic and simplest RMF Lagrangian involves the scalar-isoscalar σ and vector-isoscalar ω mesons without any interaction among themselves [81], which results in large nuclear matter incompressibility K_0 [82]. Boguta and Bodmer included a nonlinear self-coupling of the σ field which lowered the value of nuclear matter incompressibility to reasonable values. and vector-isovector ρ meson[83]. Apart from σ , ω , and ρ mesons, the addition of scalar-isoscalar δ meson is included to study the isovector effect on the scalar potential of the nucleon. Both nuclear matter and neutron star matter properties are obtained which lie well within the limits [54, 73]. The Effective field theory motivated RMF (E-RMF) is the extended RMF model which includes all possible self- and cross-couplings between the mesons [84–86]. The RMF model has gained a lot of success in investigating both finite and infinite nuclear matter properties. The various nonlinear meson coupling terms can be replaced by the density-dependent nucleon-meson coupling constants in the Density-Dependent Relativistic Hartree-Fock (DD-RHF) [87–89] and density-dependent RMF model (DD-RMF) [57]. The density-dependent models take into account the nuclear medium effect originated by the relativistic Brueckner-Hartree-Fock mode [57]. Unlike the RMF model, the coupling constants in the DD-RMF are density-dependent i.e, they vary with the density. The DD-RMF coupling constants depend either on the scalar density ρ_s or the vector density ρ_B , but the vector density parameterizations are considered usually which doesn't influence the total energy of the system.

The DD-RMF Lagrangian density is given as:

$$\begin{aligned} \mathcal{L} = \sum_{\alpha=n,p} \bar{\psi}_\alpha \left\{ \gamma^\mu \left(i\partial_\mu - g_\omega(\rho_B)\omega_\mu - \frac{1}{2}g_\rho(\rho_B)\gamma^\mu\rho_\mu\tau \right) - \left(M - g_\sigma(\rho_B)\sigma - g_\delta(\rho_B)\delta\tau \right) \right\} \psi_\alpha \\ + \frac{1}{2} \left(\partial^\mu\sigma\partial_\mu\sigma - m_\sigma^2\sigma^2 \right) + \frac{1}{2} \left(\partial^\mu\delta\partial_\mu\delta - m_\delta^2\delta^2 \right) - \frac{1}{4}W^{\mu\nu}W_{\mu\nu} \\ + \frac{1}{2}m_\omega^2\omega_\mu\omega^\mu - \frac{1}{4}R^{\mu\nu}R_{\mu\nu} + \frac{1}{2}m_\rho^2\rho_\mu\rho^\mu, \end{aligned} \quad (1)$$

where ψ_α , ($\alpha = n, p$) denotes the neutron and proton wave-function. $g_\sigma, g_\omega, g_\rho$, and g_δ are the meson coupling constants which are density-dependent, and $m_\sigma, m_\omega, m_\rho$ and m_δ are the masses for σ, ω, ρ and δ mesons respectively. The tensor fields $W^{\mu\nu}$ and $R^{\mu\nu}$ are defined as

$$\begin{aligned} W^{\mu\nu} &= \partial^\mu W^\nu - \partial^\nu W^\mu, \\ R^{\mu\nu} &= \partial^\mu R^\nu - \partial^\nu R^\mu \end{aligned} \quad (2)$$

The coupling constants of σ and ω mesons for DD-MEX, DDV, DDVT, and DDVTD parameter sets are expressed as the fraction function of the vector density. The density-dependent coupling constants for various parameterizations are given as

$$g_i(\rho_B) = g_i(\rho_0)f_i(x), \quad (3)$$

where the function $f_i(x)$ is given by

$$f_i(x) = a_i \frac{1 + b_i(x + d_i)^2}{1 + c_i(x + d_i)^2}, i = \sigma, \omega \quad (4)$$

as a function of $x = \rho_B/\rho_0$, where ρ_0 is the nuclear matter saturation density.

For the function $f_i(x)$, the number of constraint conditions defined as $f_i(1) = 1, f''_\sigma(1) = f''_\omega(1), f'_i(0) = 0$ reduce the number of free parameters from eight to three in the eq.4. Out of them, the first two constraints are

$$a_i = \frac{1 + c_i(1 + d_i)^2}{1 + b_i(1 + d_i)^2}, 3c_id_i^2 = 1 \quad (5)$$

For the isovector ρ and δ mesons, the coupling constants are given by an exponential dependence as

$$g_i(\rho_B) = g_i(\rho_0)\exp[-a_i(x - 1)] \quad (6)$$

For the DD-LZ1 parameter set, the coefficient g_i is fixed at $\rho_B=0$ for $i = \sigma, \omega$;

$$g_i(\rho_B) = g_i(0)f_i(x). \quad (7)$$

There are only four constraint conditions for σ and ω in the DD-LZ1 parameter set. The constraint $f''_\sigma(1) =$

$f''_\omega(1)$ is removed, which changes the coupling constant of ρ meson as

$$g_\rho(\rho_B) = g_\rho(0)\exp(-a_i x). \quad (8)$$

Following the Euler-Lagrange equation, we obtain the equation of motion for nucleons and mesons.

The scalar density ρ_s , baryon density ρ_B , and the isovector densities ρ_{s3} , and ρ_3 are defined as

$$\rho_s = \sum_{\alpha=n,p} \bar{\psi}\psi = \rho_{sp} + \rho_{sn} = \sum_{\alpha} \frac{2}{(2\pi)^3} \int_0^{k_\alpha} d^3k \frac{M_\alpha^*}{E_\alpha^*}, \quad (9)$$

$$\rho_B = \sum_{\alpha=n,p} \psi^\dagger\psi = \rho_p + \rho_n = \sum_{\alpha} \frac{2}{(2\pi)^3} \int_0^{k_\alpha} d^3k, \quad (10)$$

$$\rho_{s3} = \sum_{\alpha} \bar{\psi}\tau_3\psi = \rho_{sp} - \rho_{sn}, \quad (11)$$

$$\rho_3 = \sum_{\alpha} \psi^\dagger\tau_3\psi = \rho_p - \rho_n. \quad (12)$$

The effective masses of nucleons are given as

$$M_p^* = M - g_\sigma(\rho_B)\sigma - g_\delta(\rho_B)\delta, \quad (13)$$

, and

$$M_n^* = M - g_\sigma(\rho_B)\sigma + g_\delta(\rho_B)\delta \quad (14)$$

Also,

$$E_\alpha^* = \sqrt{k_\alpha^2 + M_\alpha^{*2}}, \quad (15)$$

is the effective energy of nucleon with nucleon momentum k_α . The energy-momentum tensor determines the total energy density and the pressure for the nuclear matter as

$$\begin{aligned} \mathcal{E}_{DD} &= \mathcal{E}_H + \mathcal{E}_{kin}, \\ P_{DD} &= P_H + P_{kin} \end{aligned} \quad (16)$$

where, \mathcal{E}_H and P_H are the energy density and the pressure of hadronic matter given as

$$\begin{aligned}\mathcal{E}_H &= \frac{1}{2}m_\sigma^2\sigma^2 - \frac{1}{2}m_\omega^2\omega^2 - \frac{1}{2}m_\rho^2\rho^2 + \frac{1}{2}m_\delta^2\delta^2 + g_\omega(\rho_B)\omega\rho_B + \frac{g_\rho(\rho_B)}{2}\rho\rho_3, \\ P_H &= -\frac{1}{2}m_\sigma^2\sigma^2 + \frac{1}{2}m_\omega^2\omega^2 + \frac{1}{2}m_\rho^2\rho^2 - \frac{1}{2}m_\delta^2\delta^2 - \rho_B \sum_R(\rho_B),\end{aligned}\quad (17)$$

and \mathcal{E}_{kin} and P_{kin} are the energy density and pressure from the kinetic part,

$$\begin{aligned}\mathcal{E}_{kin} &= \frac{1}{8\pi^2} \left[k_\alpha E_\alpha^* (2k_\alpha^2 + M_\alpha^2) + M_\alpha^4 \ln \frac{M_\alpha}{k_\alpha + E_\alpha^*} \right], \\ P_{kin} &= \frac{1}{24\pi^2} \left[k_\alpha E_\alpha^* (2k_\alpha^2 - 3M_\alpha^2) + 3M_\alpha^4 \ln \frac{k_\alpha + E_\alpha^*}{M_\alpha} \right].\end{aligned}\quad (18)$$

For the neutron star matter, the β -equilibrium condition is given as

$$\mu_e = \mu_\mu = \mu_n - \mu_p. \quad (19)$$

where,

$$\begin{aligned}\mu_{\alpha=n,p} &= \sqrt{k_\alpha^2 + M_\alpha^{*2}} \\ &+ \left[g_\omega(\rho_B)\omega + \frac{g_\rho(\rho_B)}{2}\rho\tau_3 + \sum_R(\rho_B) \right], \\ \mu_{l=\mu,e} &= \sqrt{k_l^2 + m_l^2}.\end{aligned}\quad (20)$$

The charge neutrality condition implies

$$q_{total} = \sum_{i=n,p} q_i k_i^3 / (3\pi^2) + \sum_l q_l k_l^3 / (3\pi^2) = 0. \quad (21)$$

To study the phase transition from hadron matter to quark matter, the Vector-Enhanced Bag model (vBag) [80] is employed which is an extension of the simple bag model [66, 71, 72]. The vBag model accounts for the Dynamic Chiral Symmetry Breaking (D χ SB) and also the additional repulsive vector interactions which allow the strange stars to achieve $2M_\odot$ limit on the maximum mass and hence satisfy the constraints from recently measured masses of pulsars like PSR J1614-2230 [30], PSR 0348+0432 [31], and PSR J0740+6620 [32].

The energy density and pressure in the vBag model follow as [90]

$$\mathcal{E}_Q = \sum_{f=u,d,s} \mathcal{E}_{vBag,f} - B_{dc}, \quad (22)$$

$$P_Q = \sum_{f=u,d,s} P_{vBag,f} + B_{dc}, \quad (23)$$

where, B_{dc} represents the deconfined bag constant introduced which lowers the energy per particle and thus favoring stable strange matter. The energy density and pressure of a single quark flavor are defined as:

$$\mathcal{E}_{vBag,f}(\mu_f) = \mathcal{E}_{FG,f}(\mu_f^*) + \frac{1}{2}K_\nu n_{FG,f}^2(\mu_f^*) + B_{\chi,f}, \quad (24)$$

$$P_{vBag,f}(\mu_f) = P_{FG,f}(\mu_f^*) + \frac{1}{2}K_\nu n_{FG,f}^2(\mu_f^*) - B_{\chi,f}, \quad (25)$$

where FG denotes the zero temperature Fermi gas. The coupling constant parameter K_ν results from the vector interactions and controls the stiffness of the star matter curve [91]. The bag constant for a single quark flavor is denoted by $B_{\chi,f}$. The chemical potential μ_f^* of the system is defined as

$$\mu_f = \mu_f^* + K_\nu n_{FG,f}(\mu_f^*). \quad (26)$$

An effective bag constant is defined in the vBag model so that the phase transition to quark matter occurs at the same chemical potential

$$B_{eff} = \sum_{f=u,d,s} B_{\chi,f} - B_{dc}. \quad (27)$$

The effective bag constant B_{eff} is an extension to the deconfined bag constant to allow the phase transition to occur at the same chemical potential. This also illustrates how the B_{eff} can be used in a two and three flavor quark matter.

The charge neutrality and β -equilibrium conditions for the quark matter are

$$\frac{2}{3}\rho_u - \frac{1}{2}(\rho_d + \rho_s) - \rho_e - \rho_\mu = 0, \quad (28)$$

$$\mu_s = \mu_d = \mu_u + \mu_e; \mu_u = \mu_e. \quad (29)$$

The density range over which a phase transition exists between hadron matter and quark matter is determined by beta-equilibrium and charge-neutral conditions [67, 92–95]. The phase transition can be either by a local charge condition (Maxwell Construction) [96] or global charge neutrality condition (Gibbs Construction) [67]. The global charge neutrality condition allows the hadron matter and the quark matter to be separately charged, unlike the local charge-neutrality condition. In this study, I used the Gibbs method to construct the hadron-quark phase transition. The global charge neutrality condition follows as

$$\chi\rho_Q + (1 - \chi)\rho_H + \rho_l = 0, \quad (30)$$

where the quark volume fraction in the mixed-phase given by $\chi = V_Q/(V_T)$ which varies from $\chi = 0$ to $\chi = 1$ in the pure hadron and pure quark phases respectively.

The charge densities of quarks, hadrons, and leptons are represented by ρ_Q , ρ_H , and ρ_l respectively.

The equations governing the mixed-phase chemical potential, pressure, energy, and the baryon density are defined as:

$$\mu_{B,H} = \mu_{B,Q}; \mu_{e,H} = \mu_{e,Q}, \quad (31)$$

and

$$P_H(\mu_B, \mu_e) = P_Q(\mu_B, \mu_e) = P_{MP}. \quad (32)$$

$$\varepsilon_{MP} = \chi\varepsilon_Q + (1 - \chi)\varepsilon_H + \varepsilon_l, \quad (33)$$

and

$$\rho_{MP} = \chi\rho_Q + (1 - \chi)\rho_H. \quad (34)$$

The above equations determine the properties of the mixed-phase and combined with the hadron equations generate overall the properties of the star.

III. NEUTRON STAR STRUCTURE AND PROPERTIES

III.1. Static neutron star

For a spherically symmetric, static neutron star, the metric element has the Schwarzschild form as ($G=c=1$)

$$ds^2 = -e^{2\phi(r)}dt^2 + e^{2\Lambda(r)}dr^2 + r^2(d\theta^2 + \sin^2\theta d\phi^2), \quad (35)$$

where the metric functions $e^{-2\phi(r)}$ and $e^{2\Lambda(r)}$ are defined as

$$e^{-2\phi(r)} = (1 - \gamma(r))^{-1}, \quad (36)$$

$$e^{2\Lambda(r)} = (1 - \gamma(r)), \quad (37)$$

with

$$\gamma(r) = 2M(r)/r \quad (38)$$

The energy-momentum tensor reduces the Einstein Field equations to well known Tolman Oppenheimer Volkoff coupled differential equations given by [97, 98]

$$\frac{dP(r)}{dr} = -\frac{[\mathcal{E}(r) + P(r)][M(r) + 4\pi r^3 P(r)]}{r^2(1 - 2M(r)/r)} \quad (39)$$

and

$$\frac{dM(r)}{dr} = 4\pi r^2 \mathcal{E}(r) \quad (40)$$

where $M(r)$ represents the gravitational mass. The boundary conditions $P(0) = P_c$, $M(0) = 0$ allows one

to solve the above differential equations and determine the properties of a neutron star.

The tidal deformability λ is defined as the ratio of the induced quadrupole mass Q_{ij} to the external tidal field \mathcal{E}_{ij} as [99, 100]

$$\lambda = -\frac{Q_{ij}}{\mathcal{E}_{ij}} = \frac{2}{3}k_2 R^5 \quad (41)$$

The dimensionless tidal deformability Λ is defined as

$$\Lambda = \frac{\lambda}{M^5} = \frac{2k_2}{3C^5} \quad (42)$$

where $C = M/R$ is the compactness parameter and k_2 is the second love number. The expression for the love number is written as [99]

$$k_2 = \frac{8}{5}(1 - 2C)^2[2C(y - 1)] \left\{ 2C(4(y + 1)C^4 + (6y - 4)C^3 + (26 - 22y)C^2 + 3(5y - 8)C - 3y + 6) - 3(1 - 2C)^2(2C(y - 1) - y + 2)\log\left(\frac{1}{1 - 2C}\right) \right\}^{-1}. \quad (43)$$

The function $y = y(R)$ can be computed by solving the differential equation [100, 101]

$$r \frac{dy(r)}{dr} + y(r)^2 + y(r)F(r) + r^2 Q(r) = 0, \quad (44)$$

where,

$$F(r) = \frac{r - 4\pi r^3[\mathcal{E}(r) - P(r)]}{r - 2M(r)}, \quad (45)$$

$$Q(r) = \frac{4\pi r \left(5\mathcal{E}(r) + 9P(r) + \frac{\mathcal{E}(r) + P(r)}{\partial P(r)/\partial \mathcal{E}(r)} - \frac{6}{4\pi r^2} \right)}{r - 2M(r)} - 4 \left[\frac{M(r) + 4\pi r^3 P(r)}{r^2(1 - 2M(r)/r)} \right]^2. \quad (46)$$

The above equations are solved for spherically symmetric and static neutron stars to determine the properties like mass, radii, and tidal deformability.

III.2. Rotating neutron stars

For a rapidly rotating neutron star with a nonaxisymmetric configuration, they would emit gravitational waves until they achieve axisymmetric configuration. The rotation deforms the neutron stars. Here we study the rapidly rotating neutron stars assuming a stationary, axisymmetric space-time. The energy-momentum tensor for such a perfect fluid describing the matter is given by

$$T^{\mu\nu} = (\mathcal{E} + P)u^\mu u^\nu + P g^{\mu\nu}, \quad (47)$$

where the first term represents the contribution from matter. u^μ denotes the fluid-four velocity, \mathcal{E} is the energy density, and P is the pressure. For rotating neutron stars, the metric tensor is given by [102–104]

$$ds^2 = -e^{2\nu(r,\theta)}dt^2 + e^{2\psi(r,\theta)}(d\phi - \omega(r)dt)^2 + e^{2\mu(r,\theta)}d\theta^2 + e^{2\lambda(r,\theta)}dr^2, \quad (48)$$

where the gravitational potentials ν, μ, ψ , and λ are the functions of r and θ only. The Einstein's field equations are solved for the given potential to determine the physical properties that govern the structure of the rotating neutron stars. Global properties like gravitational mass, equatorial radius, the moment of inertia, angular momentum and quadrupole moment are calculated.

For rotating neutron stars, the angular momentum J is easy to calculate. By defining the angular velocity of the fluid relative to a local inertial frame, $\bar{\omega}(r) = \Omega - \omega(r)$, the $\bar{\omega}$ satisfies the following differential equation

$$\frac{1}{r^4} \frac{d}{dr} \left(r^4 j \frac{d\bar{\omega}}{dr} \right) + \frac{4}{r} \frac{dj}{dr} \bar{\omega} = 0, \quad (49)$$

where $j = j(r) = e^{-(\nu+\lambda)/2}$.

The angular momentum of the star is then given by the relation

$$J = \frac{1}{6} R^4 \left(\frac{d\bar{\omega}}{dr} \right)_{r=R}, \quad (50)$$

which relates the angular velocity as

$$\Omega = \bar{\omega}(R) + \frac{2J}{R^3}. \quad (51)$$

The moment of inertia defined by $I = J/\Omega$, is given by [105, 106]

$$I \approx \frac{8\pi}{3} \int_0^R (\mathcal{E} + P) e^{-\phi(r)} \left[1 - \frac{2m(r)}{r} \right]^{-1} \frac{\bar{\omega}}{\Omega} r^4 dr, \quad (52)$$

The properties of a rotating neutron star are calculated by using the RNS code [46, 107–109].

IV. RESULTS AND DISCUSSIONS

IV.1. Parameter sets

To determine the properties of static and rotating neutron stars, we have used several recent DD-RMF parameterizations like DD-MEX [63], DD-LZ1 [62], and DDV, DDVT, DDVTD [64]. Apart from the basic DD-MEX and DD-LZ1 parameter sets, the DDV, DDVT, and DDVTD sets include the necessary tensor couplings of the vector mesons to nucleons.

Table(I) shows the necessary nucleon masses, meson masses, and the coupling constants of the used parameter sets. The meson coupling constants in the DD-LZ1

TABLE I. Nucleon and meson masses and different coupling constants for various DD-RMF parameter sets.

| | DD-LZ1 | DD-MEX | DDV | DDVT | DDVTD |
|--------------------|----------|----------|----------|----------|----------|
| m_n | 938.9000 | 939.0000 | 939.5654 | 939.5654 | 939.5654 |
| m_p | 938.9000 | 939.0000 | 938.2721 | 938.2721 | 938.2721 |
| m_σ | 538.6192 | 547.3327 | 537.6001 | 502.5986 | 502.6198 |
| m_ω | 783.0000 | 783.0000 | 783.0000 | 783.0000 | 783.0000 |
| m_ρ | 769.0000 | 763.0000 | 763.0000 | 763.0000 | 763.0000 |
| $g_\sigma(\rho_0)$ | 12.0014 | 10.7067 | 10.1369 | 8.3829 | 8.3793 |
| $g_\omega(\rho_0)$ | 14.2925 | 13.3388 | 12.7704 | 10.9871 | 10.9804 |
| $g_\rho(\rho_0)$ | 15.1509 | 7.2380 | 7.8483 | 7.6971 | 8.0604 |
| a_σ | 1.0627 | 1.3970 | 1.2099 | 1.2040 | 1.1964 |
| b_σ | 1.7636 | 1.3350 | 0.2129 | 0.1921 | 0.1917 |
| c_σ | 2.3089 | 2.0671 | 0.3080 | 0.2777 | 0.2738 |
| d_σ | 0.3799 | 0.4016 | 1.0403 | 1.0955 | 1.1034 |
| a_ω | 1.0592 | 1.3926 | 1.2375 | 1.1608 | 1.1693 |
| b_ω | 0.4183 | 1.0191 | 0.0391 | 0.04460 | 0.0264 |
| c_ω | 0.5386 | 1.6060 | 0.0724 | 0.0672 | 0.0423 |
| d_ω | 0.7866 | 0.4556 | 2.1457 | 2.2269 | 2.8062 |
| a_ρ | 0.7761 | 0.6202 | 0.3326 | 0.5487 | 0.5579 |

TABLE II. Nuclear matter properties Binding energy (E/A), incompressibility (K_0), symmetry energy (J), slope parameter (L) at saturation density for various DD-RMF parameter sets.

| | DD-LZ1 | DD-MEX | DDV | DDVT | DDVTD |
|-------------------|---------|---------|---------|---------|---------|
| $\rho_0(fm^{-3})$ | 0.158 | 0.152 | 0.151 | 0.154 | 0.154 |
| $E/A(MeV)$ | -16.126 | -16.140 | -16.097 | -16.924 | -16.915 |
| $K_0(MeV)$ | 231.237 | 267.059 | 239.499 | 239.999 | 239.914 |
| $J(MeV)$ | 32.016 | 32.269 | 33.589 | 31.558 | 31.817 |
| $L(MeV)$ | 42.467 | 49.692 | 69.646 | 42.348 | 42.583 |
| M_n^*/M | 0.558 | 0.556 | 0.586 | 0.667 | 0.667 |
| M_p^*/M | 0.5582 | 0.556 | 0.585 | 0.666 | 0.666 |

parameter set are the values at zero density while for the other parameter sets, these coupling constants are obtained at the nuclear matter saturation density ρ_0 .

Table (II) displays the nuclear matter properties like Symmetry energy, incompressibility, slope parameter at saturation density for various DD-RMF parameter sets. The binding energy E/A for all the parameter sets lies well around -16 MeV. The symmetry energy value J lies in the range 31-33 MeV which is compatible with the measurement from various astrophysical observations, $J = 31.6 \pm 2.66$ MeV [110]. The slope parameter L lies outside the constraints $L = 59.57 \pm 10.06$ MeV for the DD-LZ1 parameter set, while others satisfy this constraint properly [111, 112]. The proton and neutron effective masses are very large for DDVT and DDVTD parameter sets as compared to the DDV set.

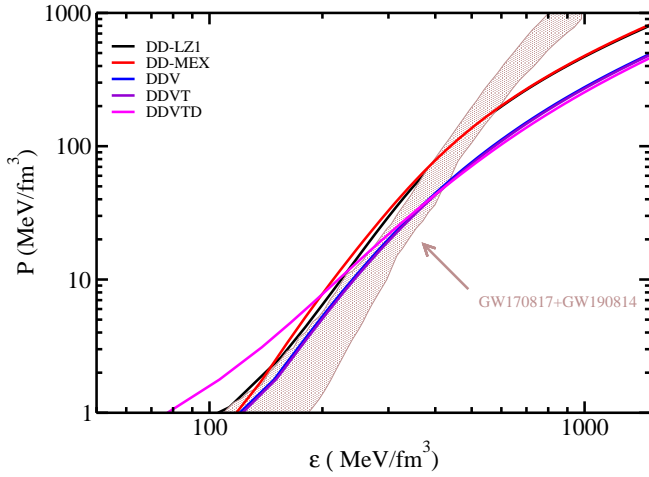


FIG. 1. (color online) Equation of State (EoS) profile for DD-LZ1, DD-MEX, DDV, DDVT, and DDVTD parameter sets. The recently combined constraints from GW170817[2] and GW190814 [4] are also shown.

IV.2. Equation of State

Fig.1 displays the various EoS for various DD-RMF parameter sets for a neutron star in beta-equilibrium and charge-neutrality conditions. The DDVTD parameter set produces the stiffest EoS at low densities and softest EoS at high density as compared to other parameter sets. DDV and DDVT sets produce soft EoS at high densities which represent a neutron star with low maximum mass. The DD-LZ1 and DD-MEX parameter sets produce stiff EoSs at high densities and hence large NS maximum mass. The recently combined constraints from the gravitational wave data GW170817 and GW190814 are also shown in the green shaded region. For a unified EoS, Baym-Pethick-Sutherland (BPS) EoS [113] is used for the outer crust part which lies in the density region 10^4 - 10^{11} g/cm³. The outer crust EoS does not effect the neutron star maximum and the radius, so we have chosen the outer crust BPS EoS for all parameter sets. The inner crust EoS has an high impact on the NS radius at the canonical mass, $R_{1.4M_\odot}$, while a small change is seen in the maximum mass and the maximum radius [114]. For the parameter sets used in this work, the inner crust EoS is not available. Thus, we have employed the DD-ME2 inner crust EoS [59] for all the parameter sets but with matching symmetry energy slope parameter [115, 116].

For the mixed-phase hadron matter and quark matter, the Gibbs Construction method, which corresponds to the global charge neutrality between two different phases, has been employed. The effective bag model with an effective bag constant $B^{1/4}$ is used to study the quark matter. The coupling constant parameter K_ν is fixed at 6 GeV^{-2} for three flavor configuration. Three different values of effective bag constant are used $B_{eff}^{1/4}=130, 145$ & 160 MeV .

Fig. (2) shows the hadron-quark phase transition with DD-RMF parameter sets for hadronic matter and vBag

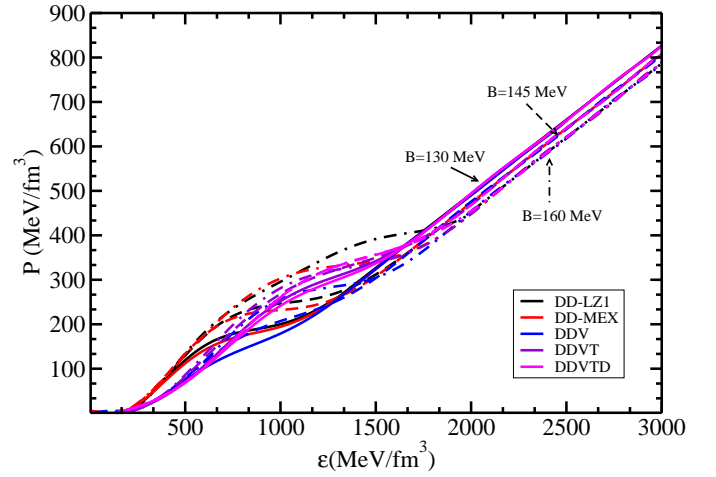


FIG. 2. (color online) Equation of state for the hadron-quark phase transition for DDV, DDVT, DDVTD, DD-LZ1, and DD-MEX hadronic parameter sets and vBag quark matter at different effective bag constants. The solid lines represent the hybrid EoS at $B_{eff}^{1/4}=130 \text{ MeV}$ while dashed and dot-dashed lines represent the hybrid EoS at $B_{eff}^{1/4}=145$ & 160 MeV , respectively.

model for quark matter using the Gibbs method for constructing mixed-phase which ensures a smooth transition between the two different phases. With the increasing effective bag constant $B_{eff}^{1/4}$, the phase transition density increases, and the mixed-phase region also expands. For bag constant $B_{eff}^{1/4}=130 \text{ MeV}$, the mixed-phase region starts from $\rho = 2.47\rho_0$ and extends upto $4.03\rho_0$. For $B_{eff}^{1/4}=145$ & 160 MeV , the mixed-phase region lies in the density range $(3.03-4.82)\rho_0$ and $(3.69-5.31)\rho_0$, respectively. DD-LZ1 and DD-MEX parameter sets produce stiff EoS and thus the mixed-phase region lies in higher pressure region than the DDV, DDVT, and DDVTD parameter sets. The mixed-phase region in the DD-LZ1 parameter sets lies in the density range $(2.56-4.23)\rho_0$ for 130 MeV , $(2.73-4.95)\rho_0$ for 145 MeV , and $(3.04-5.43)\rho_0$ for 160 MeV bag constants. Thus, DD-LZ1 and DD-MEX sets predict a large mixed-phase region as compared to the other parameter sets.

IV.3. Neutron star properties

Figure (3) displays the hadronic mass vs radius curves for DD-LZ1, DD-MEX, DDV, DDVT, and DDVTD parameter sets. The DD-LZ1 set produces an NS with a maximum mass of $2.55M_\odot$ with a radius of 12.30 km . DD-MEX set produces a $2.57M_\odot$ neutron star with a 12.46 km radius. Both these parameter sets satisfy the constraints from recent gravitational wave data GW190814 and recently measured mass and radius of PSR J0030+0451, $M = 1.34_{-0.16}^{+0.15}M_\odot$ and $R = 12.71_{-1.19}^{+1.14} \text{ km}$ by NICER [28, 117]. The DDV, DDVT, and DDVTD predict a maximum mass of $1.95, 1.93$, and $1.85 M_\odot$ for a static neutron star with radius $12.11, 11.40$, and 11.33 km

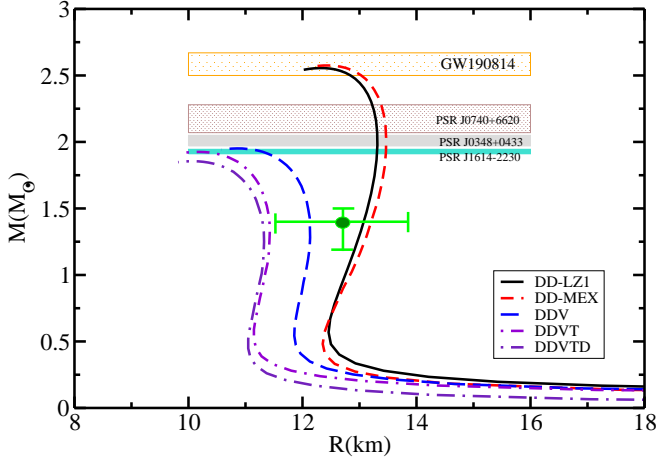


FIG. 3. (color online) Mass vs Radius profiles for pure DD-LZ1, DD-MEX, DDV, DDVT, and DDVTD parameters for a static neutron star. The recent constraints on mass from the various gravitational wave data and the pulsars are shown in the shaded region [4, 30–32] and radii [28, 117] are also shown.

at the canonical mass, $R_{1.4M_\odot}$, respectively. DDV and DDVT satisfy the mass constraint from PSR J1614-2230 and radius constraint from PSR J0030+0451. DDVTD parameter set produces a slightly lower maximum mass neutron star than PSR J1614-2230. The shaded regions display the constraints on the maximum mass of neutron star from PSR J1614-2230 ($1.928 \pm 0.017 M_\odot$) [30], PSR J0348+0432 ($2.01 \pm 0.04 M_\odot$) [31], PSR J0740+6620 ($2.14^{+0.10}_{-0.09} M_\odot$) [32], and GW190814 ($2.50\text{--}2.67 M_\odot$) [4].

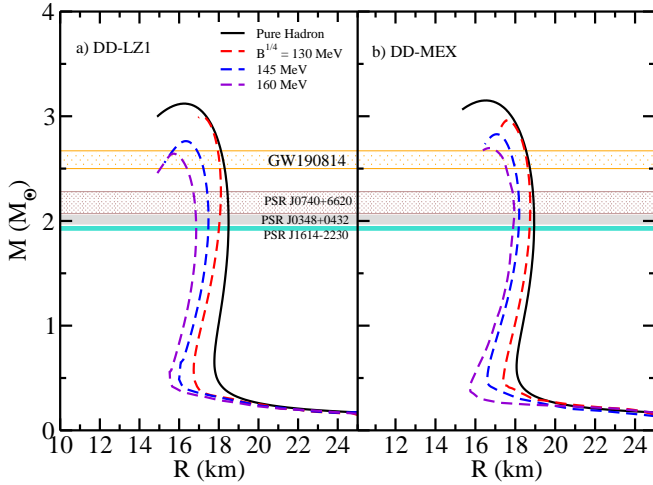


FIG. 4. (color online) Mass-Radius profile for pure hadronic and hybrid rotating neutron stars for a) DD-LZ1 and b) DD-MEX parameter sets at bag values $B_{eff}^{1/4} = 130, 145 \text{ \& } 160 \text{ MeV}$. The shaded regions represent recent constraints on the mass from various measured astronomical observables.

The rotating neutron star mass-radius profile for DD-LZ1 and DD-MEX parameter sets are shown in fig.(4). The solid lines represent the pure hadronic star while

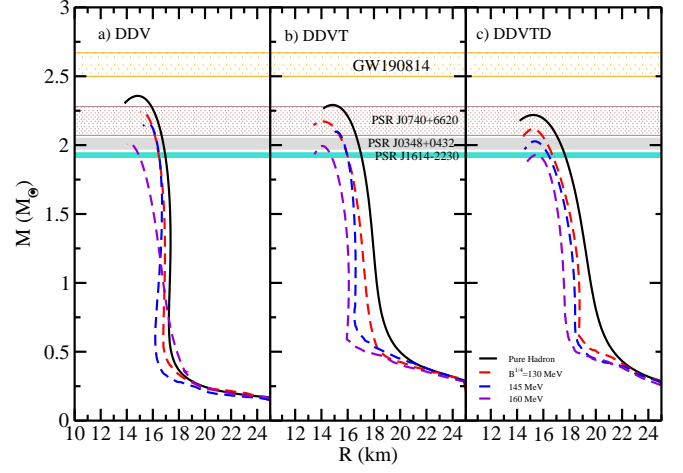


FIG. 5. (color online) Same as fig.(4), but for a) DDV, b) DDVT, and c) DDVTD EoSs.

the dashed lines represent the hybrid star at different bag constants. The effective bag constant $B_{eff}^{1/4}$ is written as $B^{1/4}$ for ease convenience. The DD-LZ1 EoS produces a pure hadronic rotating neutron star with a maximum mass of $3.11 M_\odot$ with a radius of 18.23 km. With the phase transition from hadron matter to quark matter, the maximum mass and the corresponding radius decrease with the increase in the bag constant. For DD-LZ1 set, the maximum mass decreases from $3.11 M_\odot$ to $2.98 M_\odot$ for $B^{1/4} = 130 \text{ MeV}$, and to $2.75 M_\odot$ and $2.64 M_\odot$ for $B^{1/4} = 145 \text{ \& } 160 \text{ MeV}$, respectively. The radius at the canonical mass decreases from 18.32 km for pure hadron matter to 16.64 km for hybrid star matter at 160 MeV bag value. Similarly, for the DD-MEX parameter set, the maximum mass for pure hadronic matter is $3.15 M_\odot$ at radius 16.53 km which reduces to $2.69 M_\odot$ at 16.63 km for bag constant 160 MeV. Thus while the pure hadronic rotating neutron stars predict a large maximum mass, the phase transition to quark matter lowers the maximum mass and the radius thereby satisfying the constraint from GW190814.

Figure (5) displays the mass-radius relation for hadronic and hybrid rotating neutron stars with DDV, DDVT, and DDVTD EoSs. The maximum mass for a rotating neutron star with DDV EoS is $2.37 M_\odot$ with a 17.41 km radius at the canonical mass. Both the maximum mass and the radius decrease to 2.23, 2.13, $2.01 M_\odot$ and 16.91, 16.68, 16.13 km for bag constants $B^{1/4} = 130, 145, \text{ \& } 160 \text{ MeV}$, respectively, thereby satisfying the $2 M_\odot$ constraint. For DDVT, the maximum mass reduces from 2.28 to $1.99 M_\odot$. The radius at the canonical mass also decreases from 17.82 km to 16.01 km. Similarly for DDVTD EoS, the rotating neutron star maximum mass reduces to $1.93 M_\odot$ from $2.21 M_\odot$ at $B^{1/4} = 160 \text{ MeV}$. For all the parameter sets, the phase transition to quark matter lowers the maximum mass which satisfies the $2 M_\odot$ limit.

The measurement of neutron star moment of inertia is important as it follows a universal relation with the tidal deformability and the compactness of an NS. The

moment of inertia as a function of gravitational mass for the rotating neutron stars is displayed in fig.(6). The constraint on the moment of inertia obtained from the joint PSR J0030+0451, GW170817, and the nuclear data analysis predicting $I_{1.4} = 1.43^{+0.30}_{-0.13} \times 10^{38} \text{ kg.m}^2$ is shown [118]. The predicted moment of inertia of pulsar PSR J0737-3093A, $I_{1.338} = 1.36^{+0.15}_{-0.32} \times 10^{45} \text{ g.cm}^2$ is also shown [119]. For pure hadronic matter, DD-LZ1 and DD-MEX EoSs predicts an NS with a moment of inertia 2.22 & $2.35 \times 10^{45} \text{ g.cm}^2$, respectively. The phase transition to the quark matter reduces the moment of inertia to a value 1.65 & $1.93 \times 10^{45} \text{ g.cm}^2$ for DD-LZ1 and DD-MEX parameter sets at bag constant $B^{1/4}=160 \text{ MeV}$, which satisfies the constraint from [118–120].

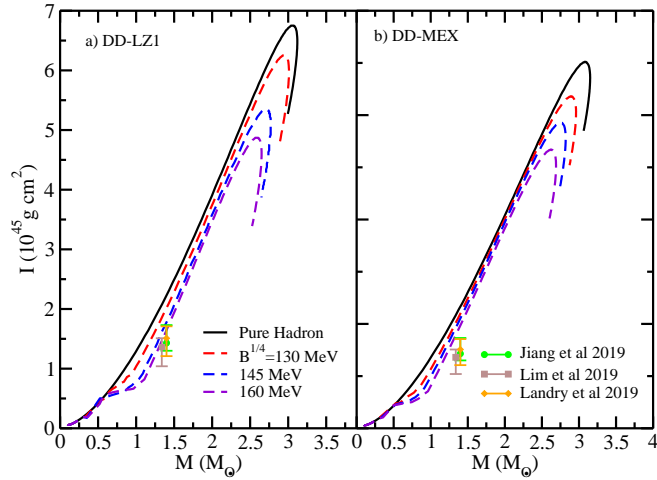


FIG. 6. (color online) Moment of inertia variation with the gravitational mass for a) DD-LZ1 and b) DD-MEX EoSs. The constraints on the moment of inertia of canonical neutron star mass are also shown [120]. The constraint from joint PSR J0030+0451, GW170817, and the nuclear data analysis are shown by green bar [118]. The predicted moment of inertia of pulsar J0737-3093A using Bayesian analysis of nuclear EoS is shown by brown bar [119].

Fig.(7) displays the moment of inertia variation with the gravitational mass for DDV, DDVT, and DDVTD parameter sets. The solid lines represent the pure hadronic matter, while the dashed lines represent the hadron-quark mixed phase at bag constants $B^{1/4}=130, 145,$ & 160 MeV . The constraints on the moment of inertia obtained from millisecond pulsars (MSP) with GW170817 universal relations are shown [121]. For DDV EoS, the moment of inertia of a pure hadronic star is found to be $2.01 \times 10^{45} \text{ g.cm}^2$ while for DDVT and DDVTD EoSs, the value is found to be 1.95 & $1.88 \times 10^{45} \text{ g.cm}^2$, respectively. For hybrid EoS, the moment of inertia is lowered to a value of $1.71 \times 10^{45} \text{ g.cm}^2$ for DDV set at bag constant 160 MeV . For DDVT and DDVTD sets, this value reduces to 1.68 & $1.64 \times 10^{45} \text{ g.cm}^2$ respectively for 160 MeV bag constant. The phase transition to quark matter

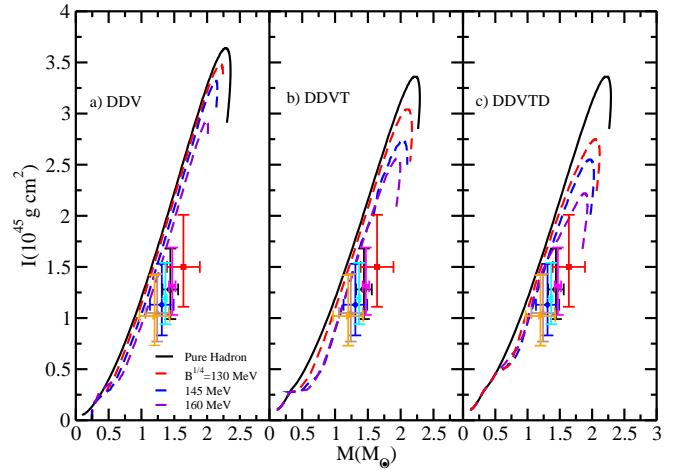


FIG. 7. (color online) Same as fig.(6) but for a) DDV, b) DDVT, and c) DDVTD parameter sets. The constraints on the moment of inertia of MSPs obtained from universal relations with GW170817 are shown [121].

produces as NS with the moment of inertia that satisfies the constraints from various measurements.

For a static neutron star, the maximum mass is usually determined as the first maximum of a $M-\varepsilon_c$ curve, i.e, $\partial M/\partial \varepsilon_c=0$, where ε_c is the central energy density. For rotating neutron stars, the situation becomes complicated. To determine the axisymmetric instability points, several methods have been used in the literature. Friedman et al. [122] described a method to determine the points at which instability is reached in rotating neutron stars [123, 124].

$$\left| \frac{\partial M(\varepsilon_c, J)}{\partial \varepsilon_c} \right|_{J=\text{constant}} = 0, \quad (53)$$

where J is the angular momentum of the star. Once the secular instability is initiated, the star evolves until it reaches a point of dynamical instability where the gravitational collapse starts [107].

The above equation defining an upper limit on the mass at a given angular momentum is sufficient but not a necessary condition for the instability. The limit on the dynamic instability is shown in ref.[125].

Figure (8) shows the variation in the gravitational mass of a rotating neutron star with the central density for DD-LZ1 and DD-MEX parameter sets. The maximum mass of $3.11M_\odot$ for DD-LZ1 EoS is produced at density $1.40 \times 10^{15} \text{ g/cm}^3$. The phase transition to quark matter at bag constant $B^{1/4}=160 \text{ MeV}$ reduces the maximum mass to $2.64M_\odot$ at $1.17 \times 10^{15} \text{ g/cm}^3$ energy density. For the DD-MEX parameter set, the maximum mass of $3.15M_\odot$ occurs at $1.47 \times 10^{15} \text{ g/cm}^3$ reduces to $2.69M_\odot$ at $1.25 \times 10^{15} \text{ g/cm}^3$. Figure (9) represents the same variation in the gravitational mass of a NS with the central density for softer EoS group (DDV, DDVT, and DDVTD).

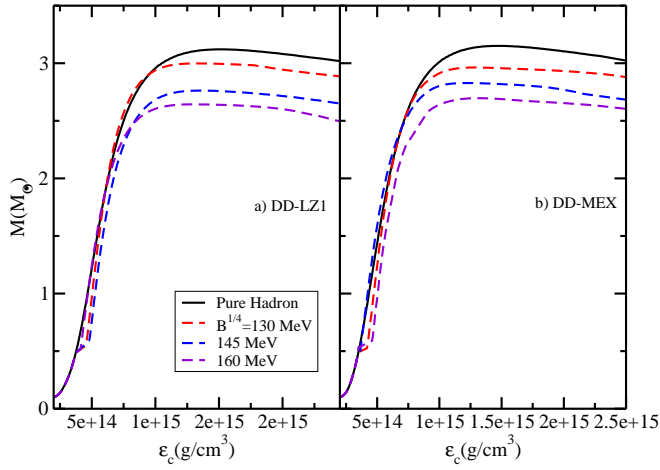


FIG. 8. (color online) Gravitational mass versus central density for a) DD-LZ1 and b) DD-MEX EoSs. The solid lines

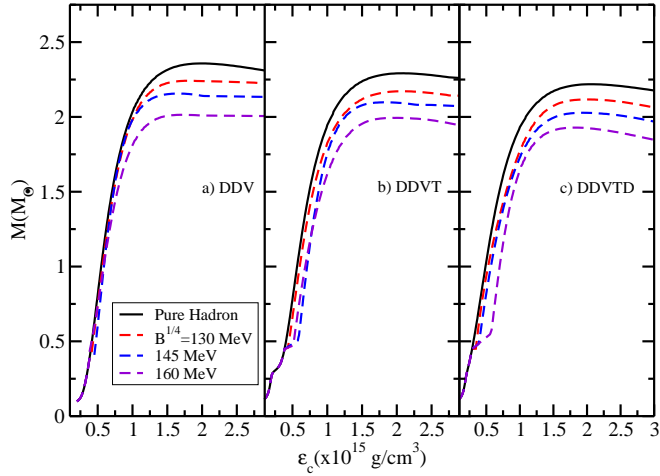


FIG. 9. (color online) Same as fig.(8) but for a) DDV, b) DDVT, and b) DDVTD EoSs.

A star rotating at a keplerian rate becomes unstable due to the loss of mass from its surface. The mass shedding limit angular velocity which is the maximum angular velocity of a rotating star is the keplerian angular velocity evaluated at the equatorial radius R_e , i.e., $\Omega_K^{J \neq 0} = \Omega_{orb}(r = R_e)$.

Figure (10) displays the neutron star gravitational mass as a function of the Kepler frequency ν_k for a) DD-LZ1 and b) DD-MEX EoSs. The limits imposed on the rotational frequency by various pulsars like PSR B1937+21 ($\nu=633$ Hz)[126], PSR J1748-2446ad ($\nu=716$ Hz)[127], and XTE J1739-285($\nu=1122$ Hz)[128] are also shown. For DD-LZ1 EoS, the pure hadronic star rotates with a maximum frequency of 1525 Hz. For hybrid star at bag value $B^{1/4}=130$ MeV, the star rotates with a frequency of 1405 Hz. For 145 and 160 bag values, the frequency obtained is 1431 and 1497 Hz, respectively.

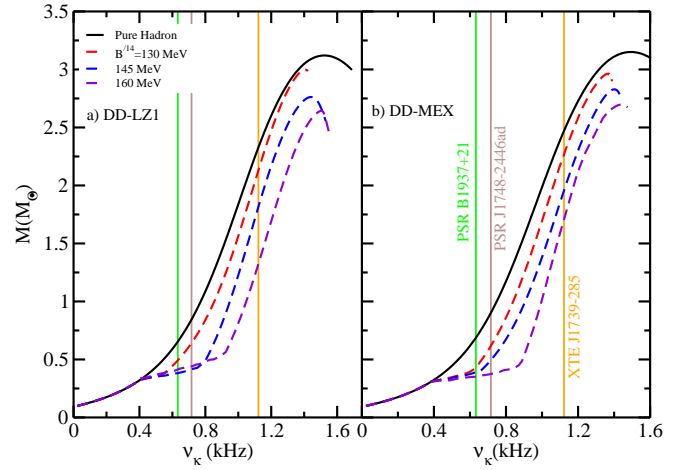


FIG. 10. (color online) Kepler frequency ν_k variation with the neutron star gravitational mass for a) DD-LZ1 and b) DD-MEX EoSs. Solid lines represent pure hadronic star while the dashed lines represent hybrid star at bag constants $B^{1/4}=130$, 145 & 160 MeV. The vertical lines represent the observational limits imposed on the frequency from rapidly rotating pulsars like PSR B1937+21 ($\nu=633$ Hz)[126], PSR J1748-2446ad ($\nu=716$ Hz)[127], and XTE J1739-285($\nu=1122$ Hz)[128].

Similarly for DD-MEX EoS, the maximum rotational frequency for a pure hadronic star is found to be 1503 Hz, which changes to 1361 Hz for the hybrid star at bag constant 130 MeV, 1408, and 1438 Hz for the hybrid star at 145 & 160 MeV bag values. Both pure hadronic and hybrid stars rotate at a frequency greater than $\nu=1122$ Hz. Also, the hybrid star $M-\nu$ curves coincide with the pure hadronic curves upto $\nu_k \approx 400$ Hz, which then show a transition towards higher frequency depending upon the bag constant.

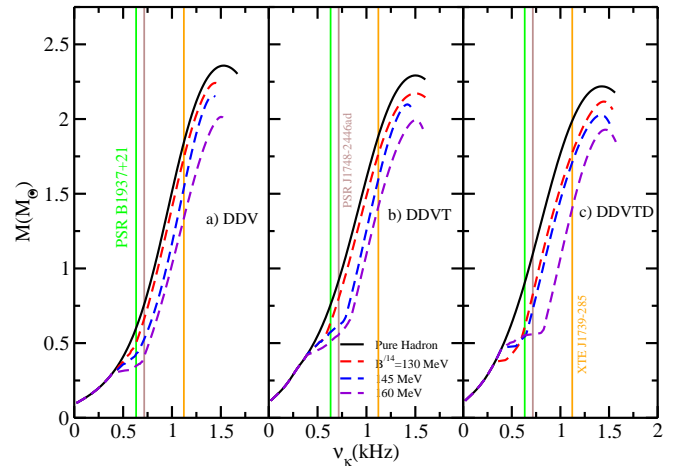


FIG. 11. (color online) Same as fig.(10) but for a) DDV, b) DDVT, and b) DDVTD EoSs.

Figure (11) displays the same gravitational mass variation with the Kepler frequency for DDV, DDVT, and

DDVTD parameter sets. For the DDV set, the pure hadronic star rotates with a rotational frequency of 1498 Hz. The hybrid stars produced with bag constants $B^{1/4}=130, 145$, and 160 MeV have a rotational frequency of 1454, 1446, and 1520 Hz, respectively. Similarly for DDVT and DDVTD EoSs, the pure hadronic star has a rotational frequency of 1473 and 1418 Hz respectively which then changes to 1503 and 1456 Hz respectively for the hybrid star at 160 MeV bag constant. Thus it is seen that the hybrid stars with a hadron-quark phase transition initially produce a low mass neutron star with a low rotating frequency than the pure hadronic star at low bag constant ($B^{1/4}=130$ MeV). By increasing the bag constant, the NS maximum mass further decreases but the rotational frequency increases. Thus the hybrid stars can withstand higher rotation as the star is denser and has low maximum mass as compared to the pure hadronic star.

A useful parameter to characterize the rotation of a star is the ratio of rotational kinetic energy T to the gravitational potential energy W , $\beta = T/W$. For a rotating neutron star, if $\beta > \beta_d$, where β_d is the critical value, the star will be dynamically unstable. The critical value β_d for a rigidly rotating star is found to be 0.27 [129, 130]. However, for different angular momentum distributions, the value lies in the range 0.14 to 0.27 [131–133].

The variation in the T/W ratio of the pure hadron and hybrid stars with the gravitational mass is shown in fig.(12). The T/W ratio for pure hadronic stars is 0.147 and 0.145 for DD-LZ1 and DD-MEX parameter sets, respectively. The hybrid stars have large T/W ratio and increase with the bag constant. For DD-LZ1 set, the ratio increases from 0.150 at $B^{1/4}=130$ MeV to 0.153 at $B^{1/4}=160$ MeV. For the DD-MEX set, the ratio increases to 0.149 and 0.151 for bag values 130 MeV and 160 MeV respectively. The large value of the T/W ratio in hybrid stars is since the quark stars are bound by strong interaction, unlike hadron stars which are bound by gravity.

Figure(13) depicts the T/W variation with the gravitational mass for DDV, DDVT, and DDVTD parameter sets. For DDV EoS, the pure hadronic star predicts a T/W ratio of 0.127, which lies below the critical value β_d . For hybrid stars, this ratio increases 0.142 for bag constant 160 MeV thereby satisfying the critical β_d limit and hence becomes dynamically unstable and emits gravitational waves. Similarly, for DDVT and DDVTD EoS, the pure hadron star produces a ratio of 0.115 and 0.108 while the hybrid star at $B^{1/4}=160$ MeV gives a value of 0.127 and 0.125, respectively.

The Einstein's field equations provide Kerr space-time for so-called Kerr black holes which can be fully described by the angular momentum J and the gravitational mass M of rotating black holes[134, 135]. The condition $J \geq GM^2/c$ must be satisfied to define a stable Kerr black hole. The gravitational collapse of massive rotating neutron stars constrained to angular momentum conservation creates a black hole with mass and angular momentum resembling that of a neutron star. Thus, it's an important quantity used in the study of black holes as

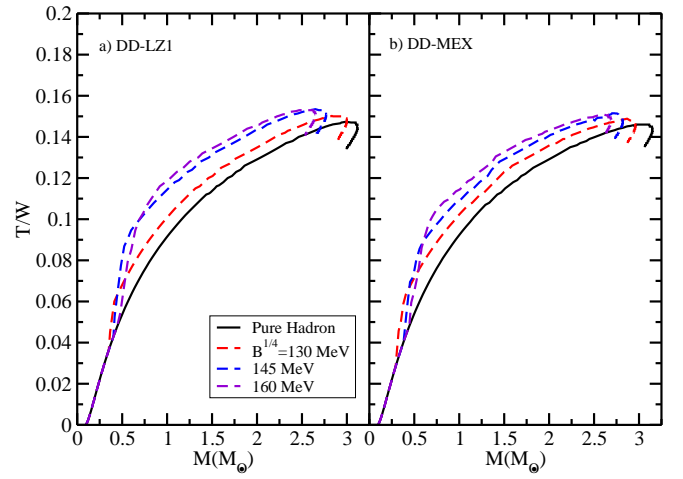


FIG. 12. (color online) Rotational kinetic energy to the gravitational potential energy ratio T/W variation with the gravitational mass for a) DD-LZ1 and b) DD-MEX EoSs. Solid lines represent pure hadronic stars while the dashed lines represent hybrid stars with bag constants $B^{1/4}=130, 145, 160$ MeV.

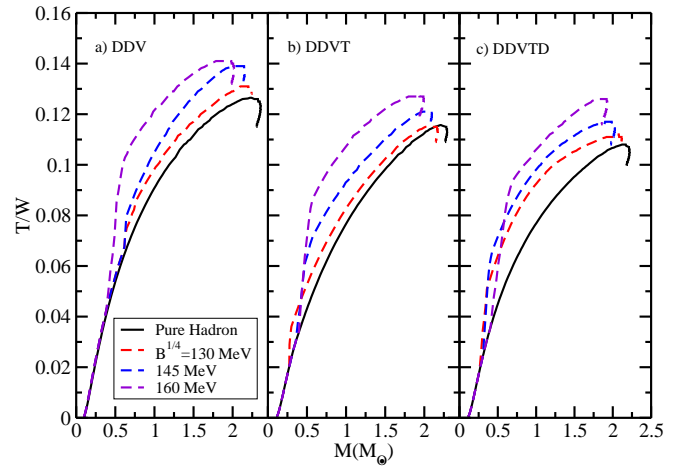


FIG. 13. (color online) Same as fig(12) but for a) DDV, b) DDVT, and c) DDVTD EoSs.

well as rotating neutron stars. The Kerr parameter leads to the possible limits on the compactness of neutron stars and also can be an important criterion for determining the final fate of the collapse of a rotating compact star [134, 136]. The Kerr parameter is described by the relation

$$\kappa = \frac{cJ}{GM^2} \quad (54)$$

where, J is the angular momentum and M is the gravitational mass of rotating neutron star. The Kerr parameter for black holes is an important and fundamental quantity with a maximum value of 0.998 [137], but it's important for other compact stars as well.

To constrain the Kerr parameter for neutron stars, we

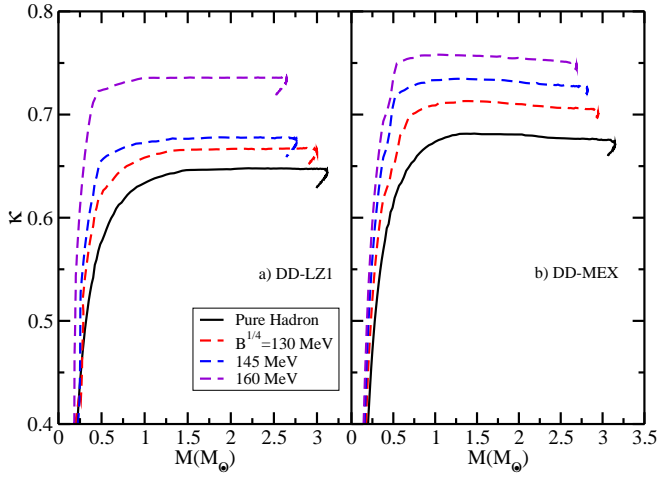


FIG. 14. (color online) Kerr parameter κ as a function of gravitational mass for a) DD-LZ1 and b) DD-MEX EoSs. The plot shows both pure hadronic stars (solid lines) and hybrid stars (dashed lines) at different bag constants.

studied the dependence of the Kerr parameter on the neutron star gravitational mass as displayed in fig.(14) and fig.(15) for the given parameter sets. From fig.(14), the Kerr parameter for pure hadronic DD-LZ1 and DD-MEX parameter sets is found to be 0.64 and 0.67 respectively. This parameter increases for the hybrid stars with a maximum value of 0.73 at $B^{1/4}=160$ MeV for the DD-LZ1 set. For the DD-MEX set, the maximum value of the Kerr parameter is 0.75 at 160 MeV bag constant. For DD-LZ1 parameter sets, the Kerr parameter remains almost unchanged once the star reaches a mass of around $1.4M_{\odot}$ for pure hadronic matter and around $1.2M_{\odot}$ for hybrid configurations. For DDV, DDVT, and DDVTD parameter sets as shown in fig.(15), the Kerr parameter value for pure hadronic stars at the maximum mass is 0.64, 0.62, and 0.61 respectively. For hybrid star configurations, the value increases to 0.75 for all parameter sets at bag constant $B^{1/4}=160$ MeV. The Kerr parameter for hybrid star configurations remains almost identical to the hadron star up to almost $0.4M_{\odot}$.

Another important quantity related to the neutron stars is the redshift which has been investigated deeply [36, 103, 138]. The measurement of redshift can impose constraints on the compactness, and in turn, on the neutron star EoS. For a rotating neutron star, if the detector is placed in the direction of the polar plane of the star, the polar redshift, also called gravitational redshift, can be measured. For a detector directed tangentially, the forward and backward redshifts can be measured. The expression for the polar redshift is given as

$$Z_P(\Omega) = e^{-2\nu(\Omega)} - 1 \quad (55)$$

where, ν is the metric function. The variation of the polar redshift with the gravitational mass is depicted in fig.(16) for DD-LZ1 and DD-MEX EoSs. For pure

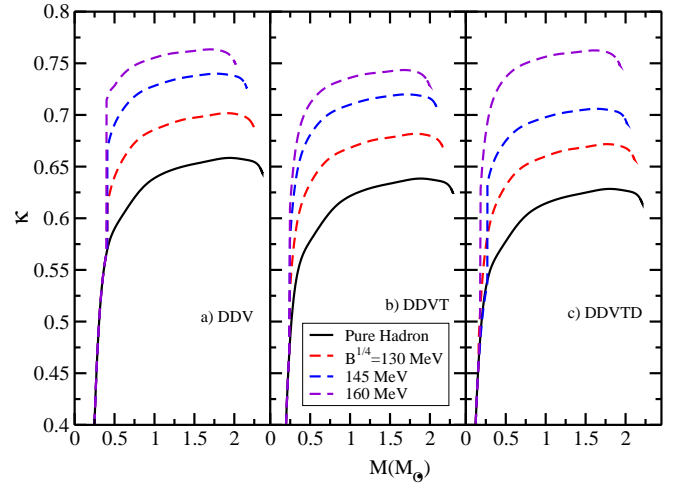


FIG. 15. (color online) Same as fig.(14) but for a) DDV, b) DDVT, and c) DDVTD EoSs.

hadronic stars, the polar redshift is found to be around 1.1 for both EoSs. With the quark matter present in the neutron stars, the polar redshift for DD-LZ1 decreases to a value 0.89, 0.84, and 0.64 for bag constants $B^{1/4}=130$, 145, & 160 MeV, respectively. Similarly for the DD-MEX set, the redshift decreases up to 0.68 for the 160 MeV bag constant. The observational limits imposed on the redshift from 1E 1207.4-5209 ($Z_P=0.12-0.23$) [139], RX J0720.4-3125 ($Z_P=0.205^{+0.006}_{-0.003}$) [46], and EXO 07482-676 ($Z_P=0.35$) [140] are also shown. The redshift prediction of $Z_P=0.35$ for EXO 07482-676 was based of the narrow absorption lines in the x-ray bursts. However, it was later seen that the spectral lines from EXO 07482-676 may be narrower than predicted [141]. Therefore the estimates of the redshift from EXO 07482-676 are uncertain.

For the softer EoS group, the polar redshift variation with the gravitational mass is shown in fig.(17) for both pure hadron matter and the hybrid star configurations. For the DDV set, the polar redshift is found to be 0.75 for pure hadronic star and decreases to 0.50 for the hybrid star at bag constant 160 MeV. For DDVT and DDVTD EoSs, the redshift decreases from 0.72 and 0.70 for pure hadron matter to 0.55 and 0.53 respectively for hybrid star at $B^{1/4}=160$ MeV. The neutron star redshift provided by measuring the gamma-ray burst annihilation lines has been interpreted as gravitationally redshifted 511 keV electron-positron pair annihilation from the neutron star surface [142]. If this interpretation is correct, then it will support an NS with redshift in the range $0.2 \leq Z_P \leq 0.5$ and thus will rule out almost every EoS studied in this work.

For the static neutron stars, the phase transition to the quark matter for DD-LZ1 and DD-MEX parameter sets is studied in ref.([62]). For DDV, DDVT, and DDVTD sets, the maximum mass obtained is around $2M_{\odot}$ and hence the phase transition to quark matter will decrease

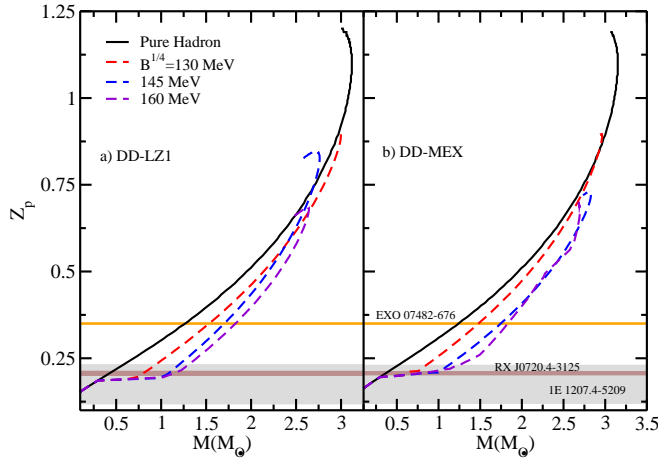


FIG. 16. (color online) Polar redshift vs gravitational mass for pure hadron and hybrid star configurations for a) DD-LZ1 and b) DD-MEX EoSs. The observational limits imposed on the polar redshift from 1E 1207.4-5209 (grey band)[139], RX J0720.4-3125 (brown band)[46] and EXO 07482-676 (yellow band)[140] are shown.

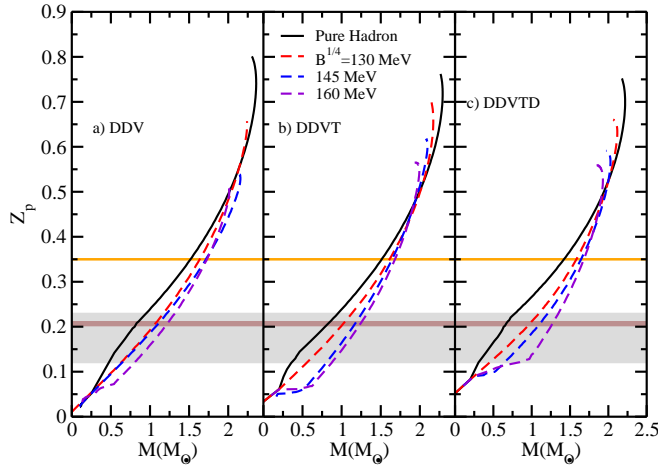


FIG. 17. (color online) Same as fig.(16) but for a) DDV, b) DDVT, and c) DDVTD EoSs.

the maximum mass to a value not satisfying any recent constraints on the mass and other neutron star properties. However, to study the properties of pure hadronic EoS, the mass-radius profile for static stars is explained above (fig.3). In addition to this, we study the tidal deformability of the given parameter sets. The equations describing the tidal deformation and its dependence on the star matter properties are described above.

The dimensionless tidal deformability Λ as a function of NS mass for the hadronic EoSs is shown in fig.(18). The constraints from the joint PSR J0030+0451, GW170817, and the nuclear data analysis at the NS canonical mass, $\Lambda_{1.4} = 370^{+360}_{-130}$ [118], and the tidal deformability of MSP obtained from GW170817 with universal relations[121] are shown. The non-parametric constraints on the tidal deformability, $\Lambda = 451^{+241}_{-279}$ is also shown[119]. The tidal deformability depends upon the

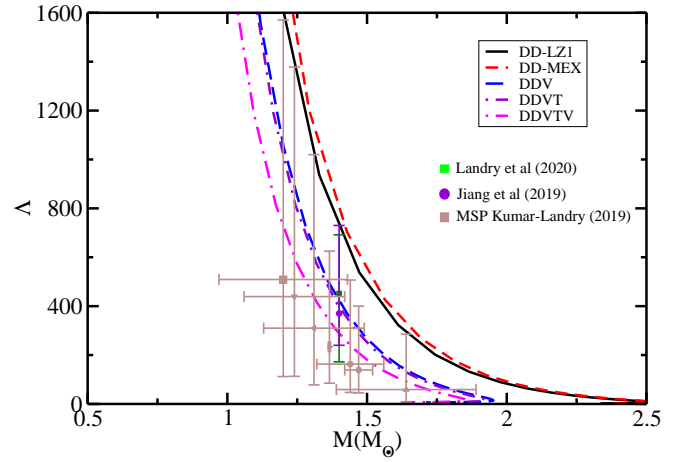


FIG. 18. (color online) Dimensionless tidal deformability as a function of NS mass for DD-LZ1, DD-MEX, DDV, DDVT, and DDVTD EoSs. The non-parametric constraints on the tidal deformability of canonical neutron star mass are shown[119]. The constraint from joint PSR J0030+0451, GW170817, and the nuclear data analysis[118], and the tidal deformability of MSP obtained from GW170817 with universal relations[121] are also shown.

NS mass and the radius. The value decreases with the increasing mass and becomes very small at the NS maximum mass. The dimensionless tidal deformability for DD-LZ1, DD-MEX, DDV, DDVT, and DDVTD EoSs at the canonical mass is found to be 727.17, 791.60, 391.23, 337.51, and 281.05, respectively. All these values lie well within the constraints defined. The DD-MEX set produces a little higher value of the tidal deformability. The value of $\Lambda_{1.4}$ for softer group EoS (DDV, DDVT, and DDVTD) is significantly lower than the stiffer group (DD-LZ1 and DD-MEX) because of the small maximum mass and the corresponding radius. However, the stiffer group EoSs cannot be neglected in comparison to the softer group. The precise measurement of the tidal deformability for the BNS mergers with a maximum mass around $2M_\odot$ by future gravitational wave detectors will lower the uncertainties in these values thereby constraining the EoSs.

V. SUMMARY AND CONCLUSION

The properties of static and rotating neutron stars are studied with a hadron-quark phase transition. The hadronic matter is studied by employing the density-dependent Relativistic Mean-Field(DD-RMF) model. Recent parameter sets like DDV, DDVT, and DDVTD along with the DD-LZ1 and DD-MEX are used to study the hadronic EoS. The quark matter is studied using a modified version of the Bag model, the Vector-Enhanced Bag model (vBag). The vBag model includes the necessary repulsive vector interactions and Dynamic Chiral Symmetry Breaking (D χ SB). The vBag model coupling parameter K_ν controlling the stiffness of the EoS

curve is held constant at 6 GeV^{-2} . The effective bag constant $B_{eff}^{1/4}$ is varied taking the values 130, 145, and 160 MeV. The Gibbs technique is used to construct the mixed-phase between hadrons and quarks which accounts for the global charge neutrality of the system. The properties like mass, radius, and the tidal deformability of static NS are studied. For rotating neutron stars, the variation in the NS properties like maximum mass, radius, the moment of inertia, rotational frequency, Kerr parameter, etc are studied in the presence of quark matter.

For static NSs, the maximum mass for the DD-LZ1 and DD-MEX is found to be 2.55 and $2.57M_{\odot}$ respectively, forming a stiffer EoS group. For DDV, DDVT, and DDVTD EoSs, the maximum is found to be around $1.9M_{\odot}$, thus lying in the softer EoS group. The phase transition properties for static NSs are not studied for the softer EoS group as it would result in a very low maximum mass not satisfying any mass constraints.

For rotating neutron stars, the maximum mass is found to be $3.11M_{\odot}$ for the DD-LZ1 set which in presence of quark matter reduces to $2.64M_{\odot}$ satisfying the recent GW190814 mass constraint. The DD-MEX set also predicts a maximum mass of $3.15M_{\odot}$ decreasing to $2.69M_{\odot}$ for $B_{eff}^{1/4}=160$ MeV bag constant. For the softer EoS group, the rotating neutron star mass lies in the range $2.2\text{--}2.3M_{\odot}$ which then reduces with the increasing bag constant to satisfy the $2M_{\odot}$ limit. The radius also decreases with the increase in the bag constant. The moment of inertia for the stiffer group lies in the range $(2.2\text{--}2.3)\times 10^{45} \text{ g.cm}^2$ for pure hadron EoSs. The phase transition to quark matter reduces the value to $1.7\times 10^{45} \text{ g.cm}^2$ satisfying the recent constraints. For the softer group of EoSs, The moment of inertia is lowered in presence of quark matter to satisfy the constraints from GW170817 with universal relations.

The variation in the rotational frequency of an NS with the gravitational mass is also studied. The pure hadronic EoSs produce NSs with high rotational frequencies. For DD-LZ1 and DD-MEX, the rotational frequency at the maximum mass is 1525 and 1503 Hz, respectively. For DDV, DDVT, and DDVTD EoSs, the frequency obtained is in the range 1400-1500 Hz. The quarks produce the hybrid star configurations with larger rotational frequencies as the quark star are more compact than hadron stars. Initially, for hybrid star configuration at $B^{1/4}=130$ MeV, the rotating with frequency smaller than a pure hadronic star is formed. As the bag constant increases, the maximum mass decreases, and the corresponding frequency increases. All the pure hadronic and hybrid star configurations produce NS with a frequency higher than the highest measured frequency of $\nu=1122$ Hz.

The ratio of rotational kinetic energy to the gravitational potential energy $\beta = T/W$ is studied to determine the dynamical stability of the rotating neutron stars. For $\beta > \beta_d (= 0.14\text{--}0.27)$, the star is considered to be dynamically unstable and hence emits gravitational radiation. The T/W ratio for rotating pure hadronic stars is found to be 0.147 and 0.145 for DD-LZ1 and DD-MEX EoSs. The quark matter phase transition tends to increase the T/W ratio with decreasing mass. For bag constant 160 MeV, the ratio is found to be 0.153 and 0.151 for DD-LZ1 and DD-MEX EoSs, respectively. For softer EoS group, this ratio lies below the critical limit for pure hadronic stars, but increases to a value well within the critical limit.

The Kerr parameter is calculated for the rotating neutron stars whose measurement allows to constrain the compactness of a star and hence EoS. The precise value of the Kerr parameter for neutron stars is not known yet, but a maximum value of 0.75 is seen in most of the theoretical works. For the given parameterization sets, the Kerr parameter value lies around 0.65 for the stiffer group and 0.6 for the softer group. Following the inverse relationship with the gravitational mass, the Kerr parameter increases in the presence of quarks. For both stiffer and softer EoS groups, the value attains a maximum value of 0.75, which remains almost unchanged as the mass increases beyond $1M_{\odot}$. The dependence of polar redshift on the NS mass is also calculated. It is seen that the polar redshift decreases in presence of quarks. The redshift parameter measured for all hybrid star configurations lies well above the predicted value from EXO 07482-676, $Z_P=0.35$.

For static, spherically symmetric stars, we have also calculated the dimensionless tidal deformability. It is seen that all the parameter sets predict a value of tidal deformability satisfying the constraints from various measurements.

Thus, it's clear that the presence of quarks inside the neutron stars affects both static and rotating star matter properties. Eliminating the uncertainties present in the values of these quantities will allow us to rule out very stiff and very soft EoSs. The measurement of tidal deformability for rotating neutron stars will help us to constraint its properties and hence determine a proper EoS in the near future. Additional gravitational-wave observations of binary neutron star mergers and more accurate measurements of other neutron star properties like mass, radius, tidal deformability will allow the universal relation-based bounds on canonical deformability to be further refined. The theoretical study of uniformly rotating neutron stars, along with the accurate measurements, may offer new information about the equation of state in high density regime. Besides, neutron stars through their evolution may provide us with a criterion to determine the final fate of a rotating compact star.

- entific Collaboration and the Virgo Collaboration), Phys. Rev. Lett. **121**, 161101 (2018).
- [3] B. P. Abbott and R. Abbott *et al.* (LIGO Scientific Collaboration and Virgo Collaboration), Phys. Rev. X **9**, 011001 (2019).
 - [4] R. Abbott and T. D. A. *et al.*, The Astrophys. Jour. **896**, L44 (2020).
 - [5] V. Dexheimer, R. O. Gomes, T. Klähn, S. Han, and M. Salinas, “Gw190814 as a massive rapidly-rotating neutron star with exotic degrees of freedom,” (2020), arXiv:2007.08493 [astro-ph.HE].
 - [6] H. Tan, J. Noronha-Hostler, and N. Yunes, “Neutron star equation of state in light of gw190814,” (2020), arXiv:2006.16296 [astro-ph.HE].
 - [7] M. Fishbach, R. Essick, and D. E. Holz, Astrophys. J. **899**, L8 (2020).
 - [8] I. A. Rather, A. A. Usmani, and S. K. Patra, “Hadron-quark phase transition in the context of gw190814,” (2020), arXiv:2011.14077 [nucl-th].
 - [9] D. A. Godzieba, D. Radice, and S. Bernuzzi, (2020), arXiv:2007.10999 [astro-ph.HE].
 - [10] E. R. Most, L. J. Papenfort, L. R. Weih, and L. Rezzolla, MNRAS **499**, L82–L86 (2020).
 - [11] N.-B. Zhang and B.-A. Li, The Astrophys. Jour. **902**, 38 (2020).
 - [12] A. Tsokaros, M. Ruiz, and S. L. Shapiro, (2020), arXiv:2007.05526 [astro-ph.HE].
 - [13] F. J. Fattoyev, C. J. Horowitz, J. Piekarewicz, and B. Reed, (2020), arXiv:2007.03799 [nucl-th].
 - [14] Y. Lim, A. Bhattacharya, J. W. Holt, and D. Pati, (2020), arXiv:2007.06526 [nucl-th].
 - [15] I. Tews, P. T. H. Pang, T. Dietrich, M. W. Coughlin, S. Antier, M. Bulla, J. Heinzel, and L. Issa, (2020), arXiv:2007.06057 [astro-ph.HE].
 - [16] M. Shibata and K. Taniguchi, Phys. Rev. D **73**, 064027 (2006).
 - [17] Y. Sekiguchi, K. Kiuchi, K. Kyutoku, and M. Shibata, Phys. Rev. Lett. **107**, 051102 (2011).
 - [18] K. Hotokezaka, K. Kiuchi, K. Kyutoku, T. Muranushi, Y.-i. Sekiguchi, M. Shibata, and K. Taniguchi, Phys. Rev. D **88**, 044026 (2013).
 - [19] A. Bauswein, T. W. Baumgarte, and H.-T. Janka, Phys. Rev. Lett. **111**, 131101 (2013).
 - [20] C. Palenzuela, S. L. Liebling, D. Neilsen, L. Lehner, O. L. Caballero, E. O’Connor, and M. Anderson, Phys. Rev. D **92**, 044045 (2015).
 - [21] S. Bernuzzi, D. Radice, C. D. Ott, L. F. Roberts, P. Mösta, and F. Galeazzi, Phys. Rev. D **94**, 024023 (2016).
 - [22] L. Lehner, S. L. Liebling, C. Palenzuela, O. L. Caballero, E. O’Connor, M. Anderson, and D. Neilsen, Class. and Quan. Grav. **33**, 184002 (2016).
 - [23] D. Radice, A. Perego, F. Zappa, and S. Bernuzzi, The Astrophys. Jour. **852**, L29 (2018).
 - [24] S. Köppel, L. Bovard, and L. Rezzolla, The Astrophys. Jour. **872**, L16 (2019).
 - [25] K. Hebeler, J. M. Lattimer, C. J. Pethick, and A. Schwenk, Phys. Rev. Lett. **105**, 161102 (2010).
 - [26] K. Hebeler, J. M. Lattimer, C. J. Pethick, and A. Schwenk, The Astrophys. Jour. **773**, 11 (2013).
 - [27] J. M. Lattimer, Annual Review of Nuclear and Particle Science **62**, 485–515 (2012), arXiv:2009.10690 [nucl-th].
 - [28] M. C. Miller, C. Chirenti, and F. K. Lamb, The Astrophys. Jour. **888**, 12 (2019).
 - [29] E. Annala, T. Gorda, A. Kurkela, J. Nättilä, and A. Vuorinen, Nature Phys. **16**, 907–910 (2020).
 - [30] P. B. Demorest, T. Pennucci, S. M. Ransom, M. S. E. Roberts, and J. W. T. Hessels, Nature **467**, 1081–1083 (2010).
 - [31] J. Antoniadis and P. C. C. Freire *et al.*, Science **340** (2013), 10.1126/science.1233232.
 - [32] H. T. Cromartie and E. Fonseca *et al.*, Nature Astronomy **4**, 72–76 (2019).
 - [33] M. Shibata, E. Zhou, K. Kiuchi, and S. Fujibayashi, Phys. Rev. D **100**, 023015 (2019).
 - [34] L. Rezzolla, E. R. Most, and L. R. Weih, The Astrophys. Jour. **852**, L25 (2018).
 - [35] B. Margalit and B. D. Metzger, The Astrophys. Jour. **850**, L19 (2017).
 - [36] G. B. Cook, S. L. Shapiro, and S. A. Teukolsky, Astrophys. J. **424**, 823 (1994).
 - [37] N. Stergioulas, L. Rev. Relativ. **1**, L19 (1998).
 - [38] V. Paschalidis and N. Stergioulas, L. Rev. Relativ. **20**, L19 (2017).
 - [39] I. A. Rather, A. A. Usmani, and S. K. Patra, J. Phys. G: Nucl. and Part. Phys. **47**, 105104 (2020).
 - [40] I. A. Rather, A. Kumar, H. C. Das, M. Imran, A. A. Usmani, and S. K. Patra, Int. J. Mod. Phys. E **29**, 2050044 (2020).
 - [41] D. D. Ofengeim, M. E. Gusakov, P. Haensel, and M. Fortin, Phys. Rev. D **100**, 103017 (2019).
 - [42] A. Sulaksono, International Journal of Modern Physics E **24**, 1550007, <https://doi.org/10.1142/S021830131550007X>.
 - [43] D. Vautherin and D. M. Brink, Phys. Rev. C **5**, 626–647 (1972).
 - [44] H. Shen, H. Toki, K. Oyamatsu, and K. Sumiyoshi, Nuclear Physics A **637**, 435 – 450 (1998).
 - [45] H. Shen, Phys. Rev. C **65**, 035802 (2002).
 - [46] Douchin, F. and Haensel, P., A&A **380**, 151–167 (2001).
 - [47] S. S. Bao and H. Shen, Phys. Rev. C **89**, 045807 (2014).
 - [48] S. S. Bao, J. N. Hu, Z. W. Zhang, and H. Shen, Phys. Rev. C **90**, 045802 (2014).
 - [49] J. D. Walecka, Ann. Phys. **83**, 491 (1974).
 - [50] C. J. Horowitz and J. Piekarewicz, Phys. Rev. Lett. **86**, 5647–5650 (2001).
 - [51] Y. Sugahara and H. Toki, Nuclear Physics A **579**, 557 – 572 (1994).
 - [52] J. Boguta and A. Bodmer, Nuclear Physics A **292**, 413 – 428 (1977).
 - [53] B. D. Serot, Physics Letters B **86**, 146 – 150 (1979).
 - [54] S. K. Singh, S. K. Biswal, M. Bhuyan, and S. K. Patra, Phys. Rev. C **89**, 044001 (2014).
 - [55] B. Kumar, S. K. Singh, B. K. Agrawal, and S. K. Patra, Nucl. Phys. A **966**, 197–207 (2017).
 - [56] B. Kumar, S. K. Patra, and B. K. Agrawal, Phys. Rev. C **97**, 045806 (2018).
 - [57] R. Brockmann and H. Toki, Phys. Rev. Lett. **68**, 3408–3411 (1992).
 - [58] T. Nikšić, D. Vretenar, P. Finelli, and P. Ring, Phys. Rev. C **66**, 024306 (2002).
 - [59] G. A. Lalazissis, T. Nikšić, D. Vretenar, and P. Ring, Phys. Rev. C **71**, 024312 (2005).
 - [60] G. A. Lalazissis, J. König, and P. Ring, Phys. Rev. C **55**, 540–543 (1997).
 - [61] H. C. Das, A. Kumar, B. Kumar, S. K. Biswal, and S. K. Patra, Phys. Rev. C **101**, 045802 (2020), arXiv:2009.10690 [nucl-th].
 - [62] B. Wei, Q. Zhao, Z.-H. Wang, J. Geng, B.-Y. Sun, Y.-F. Niu, and W.-H. Long, Ch. Phys. C **44**, 074107 (2020).
 - [63] A. Taninah, S. Agbemava, A. Afanasjev, and P. Ring, Phys. Lett. B **800**, 135065 (2020).

- [64] S. Typel and D. Alvear Terrero, *Eur. Phys. Jour. A* **56**, 160 (2020).
- [65] E. Witten, *Phys. Rev. D* **30**, 272 (1984).
- [66] E. Farhi and R. L. Jaffe, *Phys. Rev. D* **30**, 2379 (1984).
- [67] N. K. Glendenning, *Phys. Rev. D* **46**, 1274 (1992).
- [68] F. Özel, D. Psaltis, S. Ransom, P. Demorest, and M. Alford, *The Astrophys. Jour.* **724**, L199–L202 (2010).
- [69] T. Klähn, R. Lastowiecki, and D. Blaschke, *Phys. Rev. D* **88**, 085001 (2013).
- [70] I. Bombaci, D. Logoteta, I. Vidaña, and C. Providência, *Eur. Phys. Jour. A* **52**, 58 (2016).
- [71] A. Chodos, R. L. Jaffe, K. Johnson, C. B. Thorn, and V. F. Weisskopf, *Phys. Rev. D* **9**, 3471 (1974).
- [72] B. Freedman and L. McLerran, *Phys. Rev. D* **17**, 1109 (1978).
- [73] S. Kubis and M. Kutschera, *Phys. Lett. B* **399**, 191 (1997).
- [74] Y. Nambu and G. Jona-Lasinio, *Phys. Rev.* **122**, 345–358 (1961).
- [75] Y. Nambu and G. Jona-Lasinio, *Phys. Rev.* **124**, 246–254 (1961).
- [76] S. P. Klevansky, *Rev. Mod. Phys.* **64**, 649–708 (1992).
- [77] M. Buballa, *Physics Reports* **407**, 205 – 376 (2005).
- [78] C.-M. Li, J.-L. Zhang, T. Zhao, Y.-P. Zhao, and H.-S. Zong, *Phys. Rev. D* **95**, 056018 (2017).
- [79] C.-M. Li, J.-L. Zhang, Y. Yan, Y.-F. Huang, and H.-S. Zong, *Phys. Rev. D* **97**, 103013 (2018).
- [80] T. Klähn and T. Fischer, *The Astrophys. J.* **810**, 134 (2015).
- [81] C. Horowitz and B. D. Serot, *Nucl. Phys. A* **368**, 503 – 528 (1981).
- [82] J. Walecka, *Ann. Phys.* **83**, 491–529 (1974).
- [83] J. Boguta and A. Bodmer, *Nucl. Phys. A* **292**, 413–428 (1977).
- [84] R. Furnstahl, B. D. Serot, and H. B. Tang, *Nucl. Phys. A* **598**, 539 (1996).
- [85] R. Furnstahl, B. D. Serot, and H.-B. Tang, *Nucl. Phys. A* **615**, 441 – 482 (1997).
- [86] B. Kumar, S. Singh, B. Agrawal, and S. Patra, *Nucl. Phys. A* **966**, 197 – 207 (2017).
- [87] A. Bouyssy, J.-F. Mathiot, N. Van Giai, and S. Marcos, *Phys. Rev. C* **36**, 380–401 (1987).
- [88] R. Brockmann, *Phys. Rev. C* **18**, 1510–1524 (1978).
- [89] W.-H. Long, N. Van Giai, and J. Meng, *Physics Letters B* **640**, 150 – 154 (2006).
- [90] T. F. T. B. N. Cierniak, M. and Klähn, *Universe* **4**, 30 (2018).
- [91] W. Wei, B. Irving, M. Salinas, T. Klähn, and P. Jaikumar, *The Astrophys. J.* **887**, 151 (2019).
- [92] K. Schertler, S. Leupold, and J. Schaffner-Bielich, *Phys. Rev. C* **60**, 025801 (1999).
- [93] B. K. Sharma, P. K. Panda, and S. K. Patra, *Phys. Rev. C* **75**, 035808 (2007).
- [94] G. F. Burgio, M. Baldo, P. K. Sahu, and H.-J. Schulze, *Phys. Rev. C* **66**, 025802 (2002).
- [95] M. Orsaria, H. Rodrigues, F. Weber, and G. A. Contrera, *Phys. Rev. C* **89**, 015806 (2014).
- [96] D. Logoteta and I. Bombaci, *Phys. Rev. D* **88**, 063001 (2013).
- [97] R. C. Tolman, *Phys. Rev.* **55**, 364–373 (1939).
- [98] J. R. Oppenheimer and G. M. Volkoff, *Phys. Rev.* **55**, 374–381 (1939).
- [99] T. Hinderer, B. D. Lackey, R. N. Lang, and J. S. Read, *Phys. Rev. D* **81**, 123016 (2010).
- [100] B. Kumar, S. K. Biswal, and S. K. Patra, *Phys. Rev. C* **95**, 015801 (2017).
- [101] T. Hinderer, *The Astrophys. J.* **677**, 1216–1220 (2008).
- [102] E. M. Butterworth and J. R. Ipser, *Astrophys. Jour.* **204**, 200–223 (1976).
- [103] J. L. Friedman, J. R. Ipser, and L. Parker, *Astrophys. Jour.* **304**, 115 (1986).
- [104] J. L. Friedman, J. R. Ipser, and L. Parker, *Phys. Rev. Lett.* **62**, 3015–3019 (1989).
- [105] J. M. Lattimer and M. Prakash, *Physics Reports* **333–334**, 121 – 146 (2000).
- [106] A. Worley, P. G. Krastev, and B.-A. Li, *The Astrophys. Jour.* **685**, 390–399 (2008).
- [107] N. Stergioulas, *Living Rev. Relativ.* **6**, 3 (2003).
- [108] N. Stergioulas and J. L. Friedman, *‘Astrophys. Jour.* **444**, 306 (1995).
- [109] N. Stergioulas, *RNS: Rapidly rotating neutron stars* (1996).
- [110] B.-A. Li and X. Han, *Phys. Lett. B* **727**, 276 – 281 (2013).
- [111] Y. Zhang, M. Liu, C.-J. Xia, Z. Li, and S. K. Biswal, *Phys. Rev. C* **101**, 034303 (2020).
- [112] P. Danielewicz and J. Lee, *Nucl. Phys. A* **922**, 1 – 70 (2014).
- [113] G. Baym, C. Pethick, and P. Sutherland, *Astrophys. J.* **170**, 299–317 (1971).
- [114] I. A. Rather, A. A. Usmani, and S. K. Patra, (2020), [arXiv:2009.12613 \[nucl-th\]](https://arxiv.org/abs/2009.12613).
- [115] H. Pais and C. m. c. Providência, *Phys. Rev. C* **94**, 015808 (2016).
- [116] F. Grill, H. Pais, C. m. c. Providência, I. Vidaña, and S. S. Avancini, *Phys. Rev. C* **90**, 045803 (2014).
- [117] T. E. Riley, A. L. Watts, S. Bogdanov, P. S. Ray, R. M. Ludlam, S. Guillot, Z. Arzumianian, C. L. Baker, A. V. Bilous, D. Chakrabarty, K. C. Gendreau, A. K. Harding, W. C. G. Ho, J. M. Lattimer, S. M. Morsink, and T. E. Strohmayer, *Astrophys. Jour.* **887**, L21 (2019).
- [118] J.-L. Jiang, S.-P. Tang, Y.-Z. Wang, Y.-Z. Fan, and D.-M. Wei, *Astrophys. Jour.* **892**, 55 (2020).
- [119] P. Landry, R. Essick, and K. Chatziioannou, *Phys. Rev. D* **101**, 123007 (2020).
- [120] Y. Lim, J. W. Holt, and R. J. Stahulak, *Phys. Rev. C* **100**, 035802 (2019).
- [121] B. Kumar and P. Landry, *Phys. Rev. D* **99**, 123026 (2019).
- [122] J. L. Friedman, J. R. Ipser, and R. D. Sorkin, *Astrophys. Jour.* **325**, 722 (1988).
- [123] R. Sorkin, *Astrophys. J.* **249**, 254–257 (1981).
- [124] R. D. Sorkin, *Astrophys. J.* **257**, 847–854 (1982).
- [125] K. Takami, L. Rezzolla, and S. Yoshida, *MNRAS* **416**, L1–L5 (2011).
- [126] D. C. Backer, S. R. Kulkarni, C. Heiles, M. M. Davis, and W. M. Goss, **300**, 615 (1982).
- [127] J. W. T. Hessels, S. M. Ransom, I. H. Stairs, P. C. C. Freire, V. M. Kaspi, and F. Camilo, *Science* **311**, 1901–1904 (2006).
- [128] P. Kaaret, Z. Prieskorn, J. J. M. in 't Zand, S. Brandt, N. Lund, S. Mereghetti, D. Götz, E. Kuulkers, and J. A. Tomsick, *Astrophys. Jour.* **657**, L97–L100 (2007).
- [129] D. McNall, *Geophysical Journal International* **21**, 103–104 (1970).
- [130] J. E. Tohline, R. H. Durisen, and M. McCollough, *Astrophys. J.*
- [131] B. K. Pickett, R. H. Durisen, and G. A. Davis, *Astrophys. J.* **458**, 714 (1996).
- [132] J. N. Imamura, J. Toman, R. H. Durisen, B. K. Pickett, and S. Yang, *Astrophys. J.* **444**, 363 (1995).
- [133] J. M. Centrella, K. C. B. New, L. L. Lowe, and J. D.

- Brown, *Astrophys. J. Lett.* **550**, L193–L196 (2001).
- [134] K.-W. Lo and L.-M. Lin, *Astrophys. J.* **728**, 12 (2011).
 - [135] F. Cipolletta, C. Cherubini, S. Filippi, J. A. Rueda, and R. Ruffini, *Phys. Rev. D* **92**, 023007 (2015).
 - [136] P. S. Koliogiannia and C. Moustakidis, *Phys. Rev. C* **101**, 015808 (2020).
 - [137] K. S. Thorne, *Astrophys. J.* **191**, 507 (1974).
 - [138] C. Xia and W. Yong-Jiu, *Ch. Phys. Lett.* **26**, 070402 (2009).
 - [139] D. Sanwal, G. G. Pavlov, V. E. Zavlin, and M. A. Teter, *Astrophys. J.* **574**, L61–L64 (2002).
 - [140] J. Cottam, F. Paerels, and M. Mendez, *Nature* **420**, 51 (2002).
 - [141] M. Bauböck, D. Psaltis, and F. Özel, *Astrophys. J.* **766**, 87 (2013).
 - [142] E. P. Liang, *Astrophys. J.*